

Relationship between tropical cloud feedback and climatological bias in clouds

Chad W. Thackeray,^{1*} Mark D. Zelinka,² Jesse Norris,¹ Alex Hall,¹ Stephen Po-Chedley²

¹ Department of Atmospheric and Oceanic Sciences, University of California, Los Angeles, Los Angeles, California.

² Atmospheric, Earth, and Energy Division, Lawrence Livermore National Laboratory, Livermore, California.

***cwthackeray@ucla.edu**

Key Points:

- We find a relationship between tropical cloud feedback and mean-state biases in Southern Hemisphere extratropical cloud properties.
- This intermodel relationship is found to be present in three different ensembles of global climate models, a sign of robustness.
- This relationship suggests a likely tropical cloud feedback value of $0.52 \pm 0.34 \text{ W/m}^2/\text{K}$, which equates to a 34% reduction in uncertainty.

1 **Abstract**

2 Global climate model (GCM) projections of future climate are uncertain largely due to a
3 persistent spread in cloud feedback. This is despite efforts to reduce this model uncertainty
4 through a variety of emergent constraints (ECs); with several studies suggesting an important role
5 for present-day biases in clouds. Here, we use three generations of GCMs to assess the value of
6 climatological cloud metrics for constraining uncertainty in cloud feedback. We find that
7 shortwave cloud radiative properties across the Southern Hemisphere extratropics are most
8 robustly correlated with tropical cloud feedback (TCF). Using this relationship in conjunction
9 with observations, we produce an EC that yields a TCF value of $0.52 \pm 0.34 \text{ W/m}^2/\text{K}$, which
10 equates to a 34% reduction in uncertainty. Thus, we show that climatological cloud properties can
11 be used to reduce uncertainty in how clouds will respond to future warming.

12 **Plain Language Summary**

13 Different global climate models exhibit large variability in how clouds across the tropics will
14 respond to future warming. This is largely due to the complexity and diversity of responses that
15 differing cloud types may experience under warming. A long-term goal of the community has
16 been to narrow this disagreement between different models. Over the past 15 years, several
17 studies have proposed ways in which the variability in future cloud changes might be related to
18 errors in how these models represent present-day properties. Here, we use three collections of
19 models to show that variability in tropical cloud changes is closely tied to shortwave cloud
20 radiative properties across the Southern Ocean. We then use this intermodel relationship along
21 with observations to produce a best estimate of cloud feedback across the tropics.

22 **1. Introduction**

23 Global climate models (GCMs) have long disagreed about how clouds will respond to future
24 warming, as exemplified by a large and persistent intermodel spread in cloud feedback (Cess et al.
25 1990; Bony and Dufresne, 2005; Bony et al. 2006; Webb et al. 2013; Zelinka et al. 2020). Given
26 that cloud feedback is the largest source of uncertainty for model estimates of equilibrium climate
27 sensitivity (ECS) (Caldwell et al. 2016; Sherwood et al. 2020), there has been a major emphasis
28 on determining which projected cloud changes are most likely. Emergent constraints (ECs) are a
29 popular approach to tackling this problem as they use intermodel relationships between current
30 and future climate metrics in conjunction with observations to narrow uncertainty (Klein and Hall
31 2015; Williamson et al. 2021). Past studies have suggested that both observable cloud variations
32 with temperature change (Qu et al. 2014; Zhai et al. 2015; Zhou et al. 2015; Brient and Schneider
33 2016; Jiang et al. 2023) and climatological biases in cloud or radiative properties (Williams and
34 Tselioudis 2007; Volodin 2008; Trenberth and Fasullo 2010; Klein et al. 2013; Brient et al. 2016;
35 Lipat et al. 2017; Siler et al. 2018) might directly affect cloud feedback, and thus ECS.

36 Here we focus on the latter hypothesis, and briefly discuss two proposed mean-state biases

37 of relevance to global cloud feedback (GCF). Building off Volodin (2008), Siler et al. (2018) use
38 the Fifth Coupled Model Intercomparison Project (CMIP5) to find a strong relationship between
39 GCF/ECS and the difference in cloud contributions to albedo between regions of warm versus
40 cool (separated by 23.5°C isotherm) sea surface temperatures (SSTs) (derived as a projection of
41 each model's albedo climatology onto the albedo-GCF correlation map). They also show that the
42 contrast in top-of-atmosphere (TOA) shortwave cloud radiative effect (SWCRE) between these
43 two regions is a strong predictor of GCF. This study indicates that the present-day distribution of
44 clouds could inform future cloud changes through cloud albedo's dependence on SSTs and the
45 future expansion of warm SSTs. However, the physical reasoning behind the constraint has been
46 questioned (Caldwell et al. 2018).

47 Another example suggests that the present-day TOA energy balance across the Southern
48 Hemisphere (SH) is strongly tied to ECS in CMIP3 (Trenberth and Fasullo 2010). They argue that
49 GCMs with less cloud cover (and thus a more positive TOA radiative imbalance) across the
50 Southern Ocean might have greater potential for increased cloud cover in a warming climate.
51 However, this relationship was negligible in CMIP5 (Grise et al., 2015). Moreover, the CMIP3
52 relationship was found to be driven by a subset of GCMs characterized by unrealistically bright
53 present-day clouds in the SH subtropics. Instead, Grise et al. (2015) pointed to present-day cloud
54 and net radiation biases in subtropical stratocumulus-to-cumulus transition regions as important
55 for explaining ECS variability.

56 This exemplifies a common issue encountered with proposed constraints on ECS and
57 GCF: failed “out-of-sample” testing (Caldwell et al. 2018; Schlund et al. 2020), where a proposed
58 relationship is not found in a different ensemble (Hall et al. 2019). Given these difficulties,
59 several recent efforts have targeted specific cloud regimes (Qu et al. 2015; Terai et al. 2016;
60 Myers and Norris, 2016; McCoy et al. 2020; Myers et al. 2021; Hirota et al. 2021) or regions
61 (Lutsko et al. 2021; Wall et al. 2022) with the prevailing thought being that it is unlikely for a
62 single current climate metric to robustly explain uncertainty in the highly complex ECS or GCF
63 (Sherwood et al. 2020).

64 Here, we use three generations of GCMs to assess the potential value of climatological
65 cloud biases for constraining regional cloud feedbacks. We primarily focus on metrics that have
66 been shown to strongly correlate with either ECS or GCF in prior studies as these relationships
67 likely exploit some regional relationship, which happens to control intermodel spread.

68 **2. Data and Methods**

69 **2.1 Climate Models**

70 We use output from a collection of 55 GCMs from the three most recent phases of CMIP
71 (CMIP3, CMIP5, CMIP6) (Meehl et al. 2007; Taylor et al. 2012; Eyring et al. 2016) (Tables S1-

72 3). Model data comes from the first realization of the pre-industrial control (piControl), AMIP,
73 and abrupt-4xCO₂ experiments. The latter is a 150-year simulation in which the atmospheric CO₂
74 is instantaneously quadrupled from pre-industrial levels and then held fixed. The abrupt forcing
75 experiment was not run for CMIP3, so we rely on the 1pctCO₂ experiment instead. We use ECS
76 values from Zelinka et al. (2020) for CMIP5/6 and model development papers for CMIP3.

77 **2.2 Cloud Metrics**

78 Cloud feedback is calculated following Zelinka et al. (2020) for CMIP5 and CMIP6 models. First,
79 annual anomalies are computed using the abrupt-4xCO₂ experiment with respect to
80 contemporaneous 21-year running means from piControl to account for possible model drift
81 (Caldwell et al. 2016). Cloud feedback is then derived by adjusting the TOA CRE (clear-sky
82 minus all-sky upwelling flux) feedback for non-cloud effects (Soden et al. 2008; Shell et al.,
83 2008). For CMIP3, we calculate the SWCRE feedback by first computing anomalies of SWCRE
84 averaged over years 60-80 from the 1pctCO₂ experiment (surrounding the point when
85 atmospheric CO₂ has doubled) relative to the same years of piControl. These anomalies are then
86 normalized by the change in global and annual mean surface air temperature. Because these
87 CMIP3 results are not directly comparable to those of CMIP5/6, we only consider the latter when
88 building an EC on cloud feedback.

89 We also calculate several climatological cloud metrics. All climatological metrics used
90 throughout are calculated as 30-year means derived from each piControl simulation (years 100-
91 130 or the last 30 years if less than 130 years are available) and remapped to a common 2.5°x2.0°
92 grid. (Note that for AMIP results, we use the entire simulation period for each ensemble.) The
93 metrics evaluated here include SW and LW CRE at both the surface (SFC) and TOA, total cloud
94 cover (CLT), and condensed water path (CWP). TOA CRE is defined as the clear- minus all-sky
95 upwelling radiative flux at the TOA. CRE at the SFC is defined by subtracting the all- minus
96 clear-sky surface upwelling flux from the all- minus clear-sky surface downwelling flux. We will

97 primarily focus on SFC SWCRE rather than TOA because it exhibits a slightly better correlation
98 with cloud feedback, but these terms are strongly correlated across models ($r=0.96$). We assess
99 CLT because many GCMs do not provide the appropriate variables for cloud fraction at differing
100 levels of the atmosphere.

101 Lastly, we break down simulated SWCRE into contributions from cloud albedo and cloud
102 amount to interpret model biases. TOA SWCRE can be derived from the clear- and all-sky SW
103 radiative fluxes:

$$104 \quad \text{SWCRE} = \text{SW}_{\text{clr}} - \text{SW}_{\text{all}} = \text{CLT} * (\text{SW}_{\text{clr}} - \text{SW}_{\text{ov}}) \quad (1)$$

105 where SW_{ov} is the overcast SW radiative flux, which can be computed from (2).

$$106 \quad \text{SW}_{\text{all}} = \text{CLT} * \text{SW}_{\text{ov}} + (1-\text{CLT}) * \text{SW}_{\text{clr}} \quad (2)$$

107 The difference in SWCRE either between two groups or with respect to a given GCM's ensemble
108 mean can then be decomposed into two components:

$$109 \quad \Delta\text{SWCRE} = \Delta\text{CLT} * (\text{SW}_{\text{clr}} - \text{SW}_{\text{ov}}) + \text{CLT} * \Delta(\text{SW}_{\text{clr}} - \text{SW}_{\text{ov}}) \quad (3)$$

110 The first term (cloud amount contribution) is derived by holding the radiation contrast term
111 (essentially cloud albedo) constant, while the second term is derived from holding the cloud
112 fraction constant.

113 **2.3 Observational Data**

114 An observational estimate of climatological SFC SWCRE is computed from the Clouds and the
115 Earth's Radiant Energy System (CERES) dataset (Kato et al. 2018). Since surface products from
116 CERES are more uncertain than their TOA counterparts (Loeb et al. 2018), we also calculate SFC
117 SWCRE from ECMWF Reanalysis version 5 (ERA5; Hersbach et al. 2020, 2023). We use data
118 from 2001-2021 to derive these climatological means. The average of these two estimates is used
119 throughout. Since the datasets exhibit such good agreement in extratropical SFC SWCRE, we also
120 calculate annual average SFC SWCRE to quantify interannual variability in this metric. The

121 standard deviation (or the more conservative range) of these annual values is treated as
122 observational uncertainty.

123 **2.4 Constraint Methods**

124 Constrained estimates of cloud feedback are computed using the hierarchical EC framework of
125 Bowman et al. (2018). This method accounts for the correlation strength, observational
126 uncertainty, and the signal-to-noise ratio between observational and GCM uncertainty. The
127 constrained 95% prediction interval is compared to the unconstrained 95% prediction interval to
128 measure an EC's value at reducing uncertainty. We also use the EC correlation decomposition
129 method of Caldwell et al. (2018) to better understand the geographical breakdown of the
130 relationship between SH extratropical SFC SWCRE and GCF. We adapt their equation 6 as
131 follows:

$$132 \quad \text{corr}(X, GCF) = \sigma(\text{CF}_{\text{local}})/\sigma(\text{GCF}) * \text{corr}(X, \text{CF}_{\text{local}}) \quad (4)$$

133 The decomposition value at each grid cell is the product of the cross-model correlation

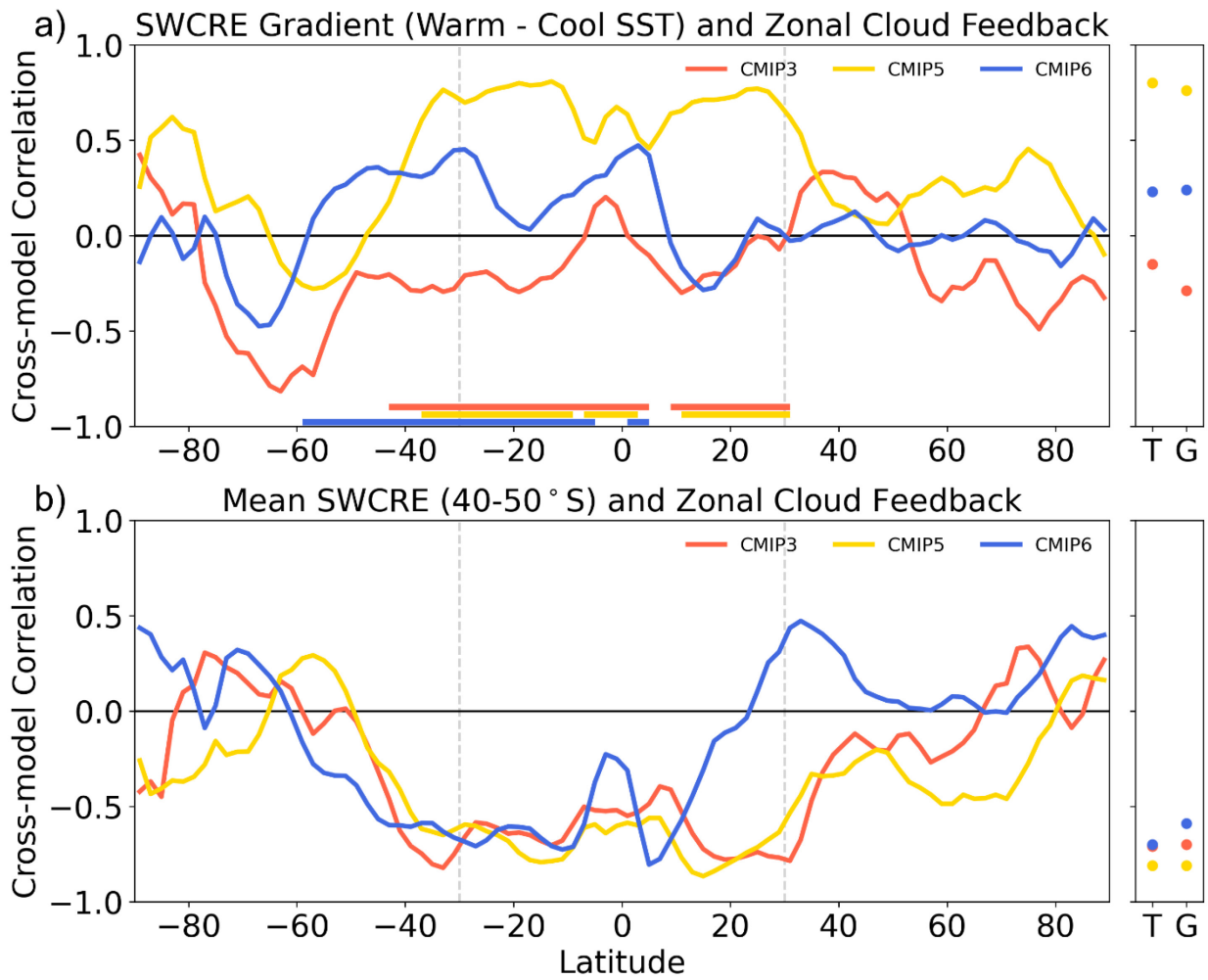
134 between a current climate metric (denoted by X) and the local cloud feedback (CF_{local}) (Fig. S1a-
135 c), and the ratio of CF_{local} variability (σ ; sampled across the ensemble) to GCF variability (Fig.
136 S1d-f).

137 **3. Results**

138 **3.1 Relevance of Climatological SFC SWCRE to Cloud Feedback**

139 We first assess how the gradient in climatological SFC SWCRE between warm and cool SST
140 regions (inspired by Siler et al. 2018) correlates with zonal-mean cloud feedback across three
141 CMIP generations (Fig. 1a). It is important to gauge EC robustness using multiple ensembles
142 because a relationship can appear in a single ensemble by chance (Caldwell et al. 2014) and large
143 changes can occur from one ensemble to the next (Schlund et al. 2020; Text S1; Fig. S2). Strong
144 correlations are evident over 40°S-30°N for CMIP5, which is expected since this EC was
145 developed on CMIP5. These latitudes also happen to coincide with regions where zonal-mean

146 cloud feedback is strongly correlated ($r>0.7$) with GCF (illustrated by bars along the x-axis of Fig.
 147 1a). Because of this, the gradient metric is strongly correlated with both the tropical cloud
 148 feedback (TCF; defined as 30°S - 30°N ; $r=0.80$) and GCF ($r=0.76$). However, we find substantially
 149 weaker correlations in both CMIP3 ($r=-0.15$ for TCF, -0.29 for GCF) and CMIP6 ($r=0.23$ for
 150 TCF, 0.24 for GCF). Cross-model correlation maps show that this weakening is tied to a less
 151 positive, or even negative, correlation between SWCRE across warm SST areas and TCF in
 152 CMIP3 and CMIP6 (Fig. 2a-c). Moreover, in CMIP6, there is a southward shift in which latitudes
 153 are driving variability in GCF, whereby 40 - 60°S plays a more important role (Fig. 1a). These
 154 latitudes are also more important for ECS variability in CMIP6 (Lutsko et al. 2021).



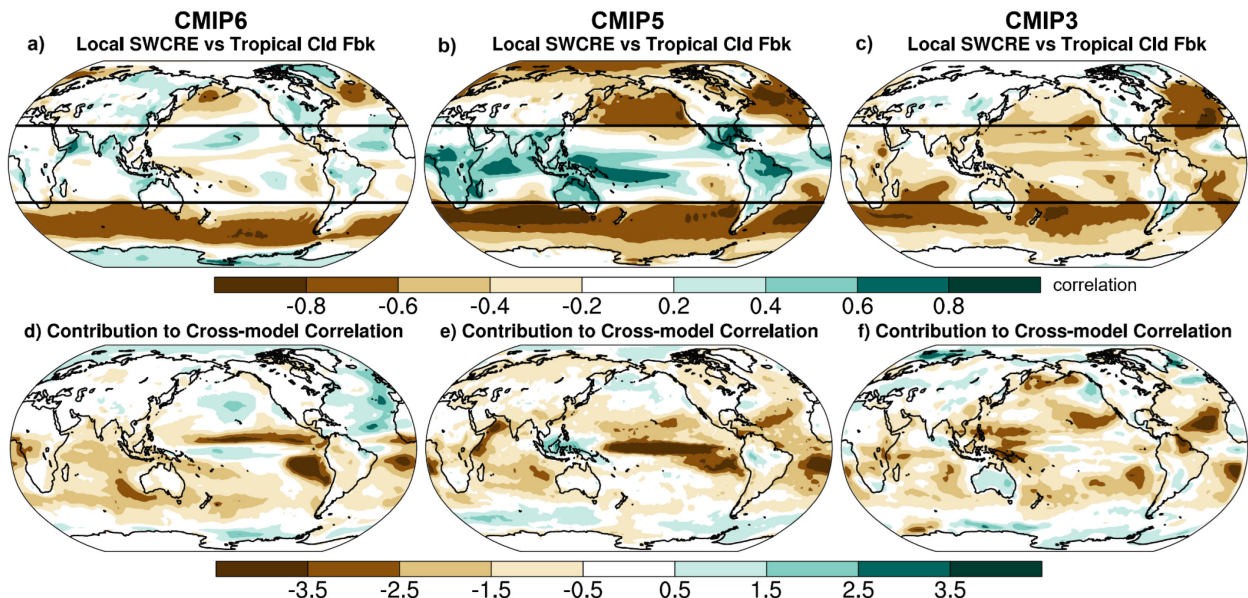
155
 156 **Fig. 1.** Cross-model correlation between zonal-mean cloud feedback and (a) the gradient in SFC SWCRE between
 157 areas of warm and cool SSTs inspired by Siler et al (2018), (b) the mean SFC SWCRE over 40 - 50°S . Individual
 158 colored lines represent the results for each of the CMIPs. Latitudes where zonal-mean cloud feedback is strongly

159 correlated ($r>0.7$) with GCF are illustrated on panel a by horizontal bars along the x-axis. Cross-model correlations
160 between these metrics and TCF/GCF are also shown on the right panel of each plot as colored dots.

161 Building off prior work which suggests potential connections between SH radiative fluxes
162 to GCF and ECS (Trenberth and Fasullo 2010; Grise et al. 2015), we also evaluate the relevance
163 of SWCRE across the SH to zonal-mean cloud feedback. We find that 40-50°S SFC SWCRE is
164 strongly tied to cloud feedback across much of the 40°S-20°N range in all three ensembles (Fig.
165 1b). This manifests as a strong negative correlation with TCF, with correlations ranging from -
166 0.70 in CMIP6 to -0.81 in CMIP5. Because these latitudes tend to control a substantial portion of
167 intermodel variability in GCF, there is also a strong correlation with GCF in CMIP3 ($r=-0.70$) and
168 CMIP5 ($r=-0.81$). The CMIP6 result is slightly weaker ($r=-0.59$) given a greater role for the SH
169 mid-latitudes in controlling GCF and less negative correlations at the equator and north of 15°N.
170 Weaker equatorial correlations stem from two anomalous GCMs, while the decline polewards of
171 15°N is driven by weak feedbacks in the CESM2 models (Fig. S3). (Note that similar analysis
172 was performed for a variety of other metrics (LWCRE, TOA SWCRE, CLT, CWP, and TOA
173 albedo; Fig. S4) and latitude bands (Fig. S5), but this is not discussed for brevity).

174 Given the robustness of the 40-50°S SFC SWCRE relationships, this will be our focus
175 going forward. Cross-model correlation maps emphasize that a strong anti-correlation between
176 TCF and SFC SWCRE over mid-latitude ocean basins is the main persistent feature of this
177 relationship across generations (Fig. 2a-c). This relationship is particularly robust in the SH,
178 where climatological cloud cover is very large (Grise et al. 2015; Kay et al. 2016). We can better
179 understand the relationship between 40-50°S SFC SWCRE and GCF using the correlation
180 decomposition framework of Caldwell et al. (2018). This method dissects cross-model
181 correlations to quantify the contribution of a specific region (see Methods). It considers both the
182 cross-model correlation between 40-50°S SFC SWCRE and the local cloud feedback (Fig. S1a-c),
183 and the ratio of local cloud feedback variability to GCF variability (Fig. S1d-f). The
184 decomposition shows large-scale consistency across model generations: larger climatological 40-

185 50°S SWCRE corresponds to greater local cloud feedback throughout the tropics (Fig. 2d-f).
186 Regions with important low cloud feedback off the west coasts of South America, Africa, and
187 Australia contribute to the negative correlation, but the magnitude and precise locations vary by
188 ensemble.

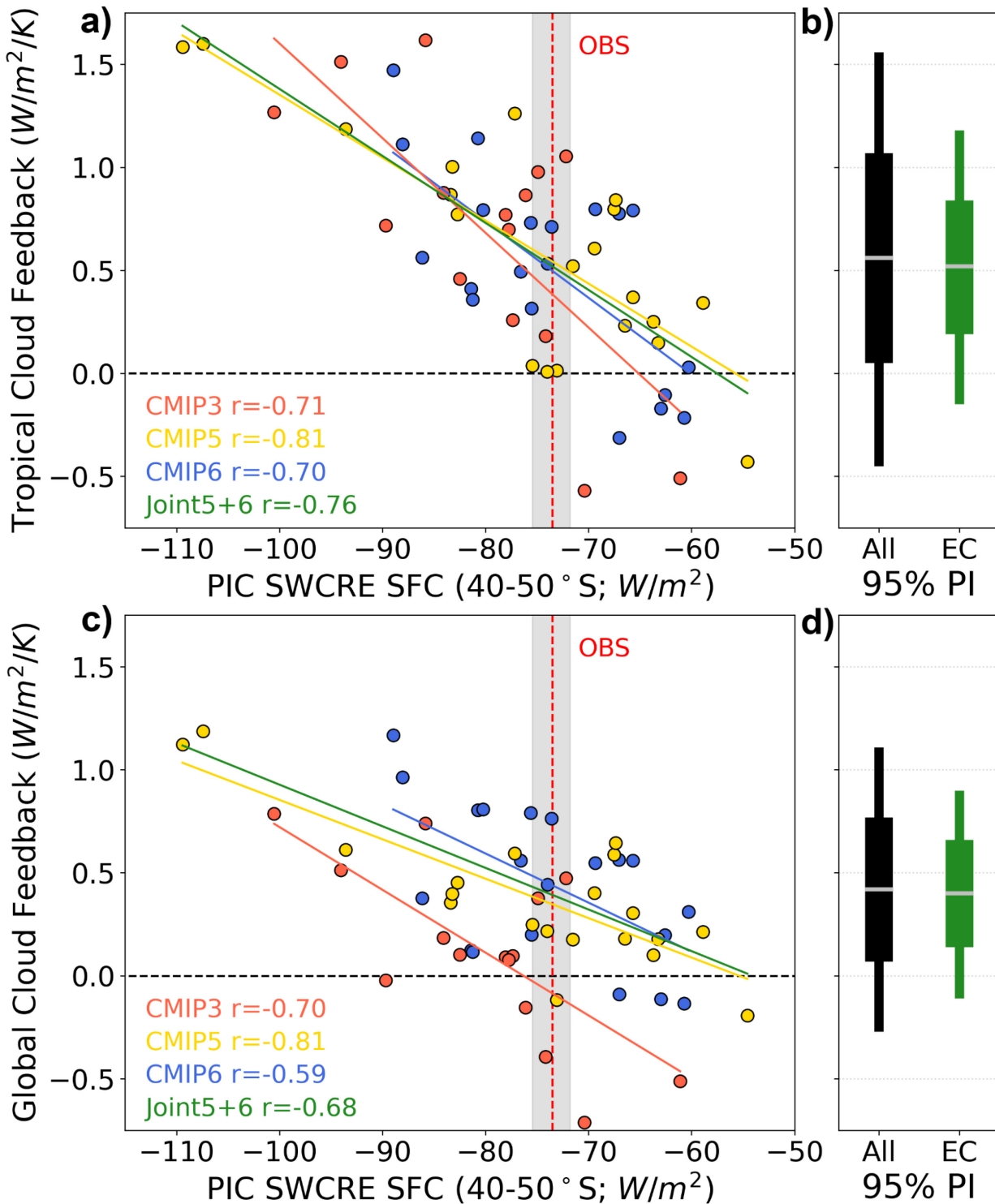


189
190 **Fig. 2.** Cross-model correlation maps between local SFC SWCRE and TCF for (a) CMIP6 (b) CMIP5 (c) CMIP3.
191 Regionally decomposed cross-model correlation (see Methods) for the relationship between 40-50°S SFC SWCRE
192 and GCF following Caldwell et al. (2018) for (d) CMIP6 (e) CMIP5 (f) CMIP3. The local contribution values can be
193 spatially averaged to obtain the correlation shown in Figure 2b. Solid black lines denote the tropical region (30°S-
194 30°N).

195 3.2 Emergent Constraint on Tropical Cloud Feedback

196 Given the robustness of this relationship, we build an EC on TCF. In Figure 3a we scatter
197 climatological SFC SWCRE averaged across 40-50°S against the TCF. (Note that these
198 climatological values are very similar in magnitude and strongly correlated with those derived
199 from historical and AMIP simulations). For reference, we also show the relationship with GCF
200 (Fig. 3c). Observations from CERES and ERA5 over 2001-2021 are used in conjunction with this
201 relationship to form the EC. We derive an estimate of observational uncertainty from interannual
202 variability. The observed estimate ($-73.5 \pm 0.8 \text{ W/m}^2$; [66% confidence interval]) suggests that
203 GCMs tend to be negatively biased when it comes to SH mid-latitude SFC SWCRE (average of

204 all GCMs: $-76.1 \pm 11.6 \text{ W/m}^2$). CMIP3 is the most consistently negatively biased (-79.9 ± 9.9
 205 W/m^2), signaling that some progress has been made. However, because the CMIP3 cloud
 206 feedback values are not derived in the same way as for CMIP5/6 (see Methods), we exclude this
 207 data when building the EC. Given the similar slopes for each ensemble, we only report results for
 208 a combined ensemble of CMIP5 and CMIP6 (individual ensemble results are in Text S2).



210 **Fig. 3.** Scatterplot of climatological SFC SWCRE averaged over 40-50°S versus (a) TCF, (c) GCF where each point
211 represents a different GCM. The vertical dashed red line represents an observed estimate from observations (CERES,
212 ERA5) while grey shading denotes the range in annual mean values, which is used in the derivation of the EC (see
213 Methods). (b) 95% prediction interval of TCF for the unconstrained CMIP5/6 ensemble (black) and the EC (green).
214 (d) same as b but for the GCF. The horizontal grey dash denotes the central estimate for each dataset, while the wider
215 portion of the bar shows the 66% prediction interval.

216 The EC yields a TCF value of $0.52 \pm 0.34 \text{ W/m}^2/\text{K}$, which represents a 34% reduction in

217 the likely range of TCF (Fig. 3b). We use a conservative 95% prediction interval (PI) derived

218 from the hierarchical EC framework (Bowman et al. 2018) to measure the uncertainty reduction

219 (see Methods). The central estimate of TCF is slightly reduced from the unconstrained ensemble

220 ($0.56 \pm 0.51 \text{ W/m}^2/\text{K}$). This constraint is also slightly weaker than a prior estimate using monthly

221 and annual CRE-based tropical cloud variability metrics to constrain TCF (90% confidence

222 interval of $-0.22\text{--}1.39 \text{ W/m}^2/\text{K}$; Lutsko et al. 2021). For reference, we also show the resulting EC

223 for GCF (Fig. 3d), which exists because of the key role that the tropics play in driving GCF

224 spread (Fig. S1d-f). This constraint suggests a GCF value of $0.40 \pm 0.26 \text{ W/m}^2/\text{K}$, which

225 represents a 26% reduction in the likely range compared to the unconstrained ensemble ($0.42 \pm$

226 $0.35 \text{ W/m}^2/\text{K}$). Our constrained GCF estimate also agrees well with the two most notable

227 community assessments in recent years (Sherwood et al. 2020: $0.45 \pm 0.33 \text{ W/m}^2/\text{K}$; Forster et al.

228 2021: $0.42 \pm 0.30 \text{ W/m}^2/\text{K}$).

229 **3.3 Investigating Drivers of Model Spread**

230 To better understand the relationship between 40–50°S SFC SWCRE and TCF, we group GCMs

231 by their 40–50°S SFC SWCRE (ten highest and ten lowest across CMIP3/5/6; Tables S1-3) and

232 assess differences in the subsequent group averages. As per the emergent relationship, the Group

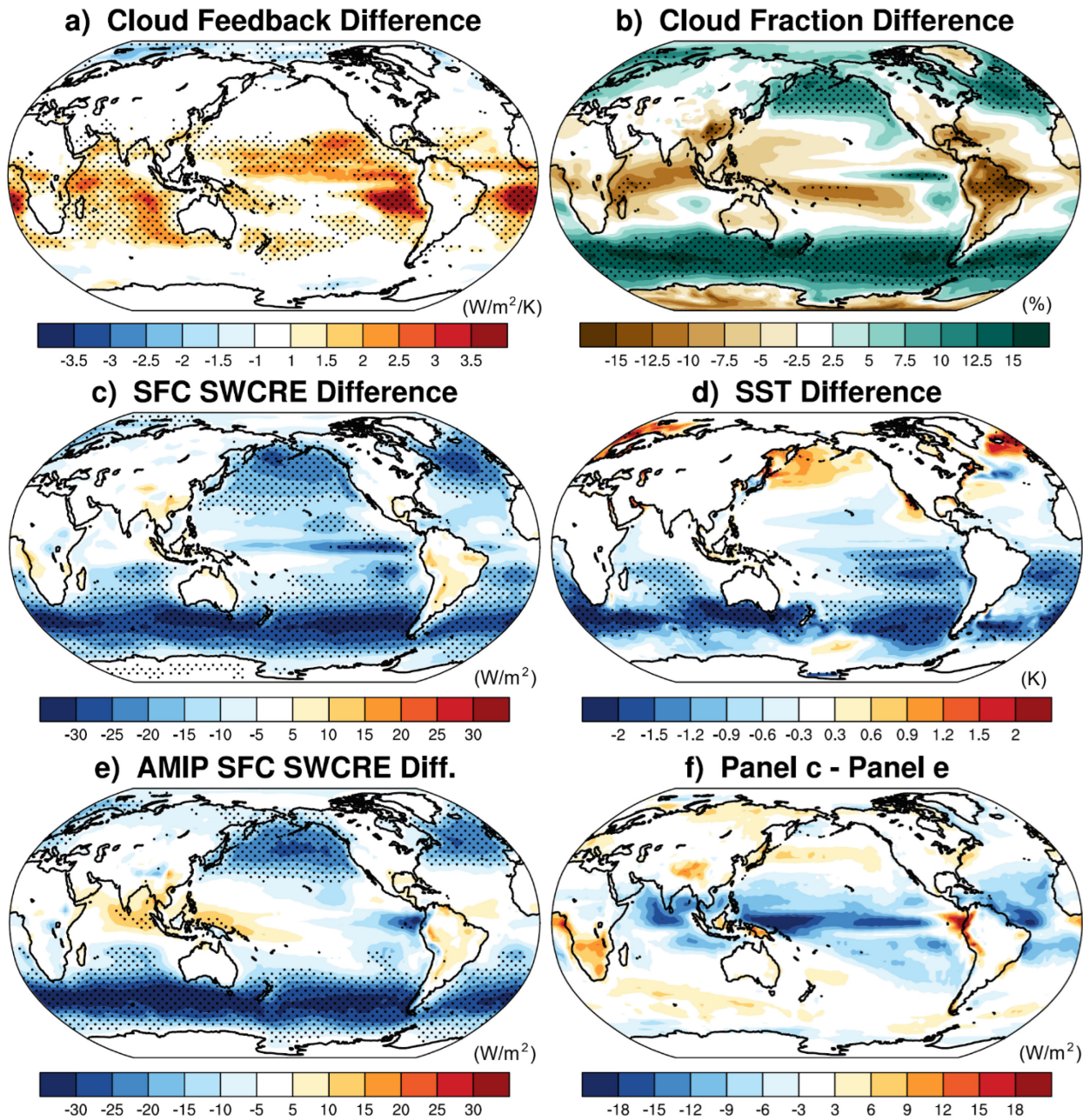
233 1 models (more negative SFC SWCRE) exhibit much stronger cloud feedback than their Group 2

234 counterparts (less negative SFC SWCRE) (Fig. 4a). In terms of GCF, their group means are 0.74

235 $\text{W/m}^2/\text{K}$ and $0.04 \text{ W/m}^2/\text{K}$, respectively. This discrepancy stems from the tropics, where the

236 difference between group means is even larger ($1.26 \text{ W/m}^2/\text{K}$, $-0.03 \text{ W/m}^2/\text{K}$). This contributes to
 237 large differences in ECS as well (4.35 vs 2.85K). It has been hypothesized that high ECS models
 238 simulate too many stratocumulus clouds in regions dominated by cumulus clouds, thus producing
 239 a stronger response of low clouds to warming (Cesena and Del Genio, 2021). However, CMIP
 240 output does not let us assess these cloud types.

Group 1 Mean - Group 2 Mean



241
 242 **Fig. 4.** Maps of the difference in (a) cloud feedback, (b) climatological total cloud fraction, (c) climatological SFC
 243 SWCRE, and (d) climatological sea surface temperatures between two groups of GCMs defined based on their

244 climatological 40-50°S SFC SWCRE. Group 1 models have a more negative SFC SWCRE than group 2. (e) same as
245 panel c but derived from AMIP simulations, (f) influence of coupling on the SFC SWCRE difference between the
246 two groups. Stippling indicates areas of statistical significance determined using a t-test ($p < 0.05$).

247 We find that Group 1 models consistently have greater CLT across extratropical oceans
248 (Fig. 4b), which is surprising given that Group 2 contains more CMIP6 models (4/10 vs. 3/10),
249 and that CMIP6 has systematically increased CLT relative to CMIP5 (Fig. S2). Moreover, while
250 Group 1 models by definition have more negative extratropical SFC SWCRE, this discrepancy
251 also extends to parts of the tropical oceans (Fig. 4c), particularly where cloud feedback
252 differences are large (Fig. 4a). Group 1 contains more CMIP3 models, which exhibit
253 unrealistically bright clouds in the SH subtropics, but similar results hold when CMIP3 is
254 excluded (Fig. S6). SWCRE differences largely coincide with Group 1 models exhibiting cooler
255 climatological sea surface temperatures (SSTs) across much of the SH and particularly the
256 southeast Pacific (Fig. 4d), conditions that favor greater low-level cloud development (Mechoso
257 et al. 2016). Since similar SFC SWCRE differences are also apparent in AMIP simulations (Fig.
258 4e), these cooler SSTs are likely driven partly by more negative SFC SWCRE, rather than vice
259 versa. Fully coupled simulations even enhance SFC SWCRE differences in tropical low-cloud
260 regions (Fig. 4f). These results agree with past work, which shows that through radiative
261 perturbation experiments, extratropical energy biases can influence mean-state tropical SSTs and
262 clouds (Mechoso et al. 2016; Kang et al. 2020; Kang et al. 2023).

263 **3.4 Discussion of Mechanisms**

264 The physical mechanisms driving the relationship between climatological SH extratropical SFC
265 SWCRE and TCF are complex, but we offer some speculation for why this relationship exists. As
266 suggested above, SH extratropical SWCRE affects tropical low clouds through a teleconnection
267 likely via the southeast Pacific. Kim et al. (2022) hypothesize that SH extratropical cooling
268 propagates into the subtropics and is advected further equatorward by climatological winds. This
269 cooling is then enhanced by a series of processes including the wind-evaporation-SST feedback,

270 stratocumulus cloud feedback, and coastal upwelling. We find that GCMs with more negative 40-
271 50°S SWCRE tend to exhibit more negative SWCRE and cooler SSTs across tropical low cloud
272 areas (Fig. 4). These cooler conditions likely help promote greater, more reflective climatological
273 low clouds in the tropics. In fact, the presence of brighter clouds in Group 1 models becomes
274 evident across most latitudes when the SWCRE difference between Groups 1 and 2 is
275 decomposed into contributions from cloud amount and albedo (Fig. S7; see Methods). Therefore,
276 when these brighter clouds are subjected to future warming, which promotes the loss of low
277 clouds, the GCM produces a stronger cloud feedback (Fig. 4a). Notably, the Group 1 models also
278 feature a slightly stronger reduction in tropical CLT (-4.3% compared to -1.3% in Group 2).

279 In contrast to the SH extratropics, mean-state tropical cloud properties are subject to a
280 variety of influences that mask any relationship with TCF (Fig. 2a-c). For instance, the cloud
281 brightness differences noted previously are counteracted by greater cloud amount across the
282 tropics in Group 2 models. This contrasts with the SH, where cloud amount differences enhance
283 the cloud brightness discrepancy. Moreover, this disconnect between SFC SWCRE and cloud
284 feedback locally is likely exacerbated by large intermodel differences in tropical cloud coverage
285 (e.g., in location and extent; Fig. S8) as CLT and SWCRE exhibit their best agreement in low
286 cloud areas (Fig. S8e). Lastly, the idea that SH extratropical cloud properties are relevant to
287 tropical clouds is supported by a moderate correlation between 40-50°S SWCRE in CMIP5-6
288 with two climatological cloud metrics computed across the tropics (deseasonalized monthly and
289 annual CRE sensitivities) from Lutsko et al. (2021) (Fig. S9).

290 **4. Conclusions**

291 Using climatological biases for ECs is a potentially promising avenue for research as it gives
292 modeling centers a relatively easy target metric to monitor during development stages. Here, we
293 use three ensembles of GCMs to explore the potential of using climatological biases in clouds for
294 constraining regional cloud feedback. We find the greatest value in climatological SFC SWCRE

295 across the SH mid-latitudes (40-50°S), which is strongly tied ($|r| \geq 0.7$) to TCF in all generations.
296 Using this relationship in conjunction with observations, we produce an EC on TCF, which
297 suggests a TCF of $0.52 \pm 0.34 \text{ W/m}^2/\text{K}$, compared to the unconstrained estimate of 0.56 ± 0.51
298 $\text{W/m}^2/\text{K}$. This suggests that the model mean is slightly too strong, while also representing a 34%
299 reduction in model uncertainty. Given the importance of the tropics to GCF, 40-50°S SFC
300 SWCRE can also be used to infer a GCF value of $0.40 \pm 0.26 \text{ W/m}^2/\text{K}$, which agrees well with
301 two notable community assessments (Sherwood et al. 2020; Forster et al. 2021).

302 Past research identified various metrics as potentially relevant to variability in TCF/GCF.
303 This includes parametric differences in extratropical mixed phase cloud partitioning (McCoy et al.
304 2016). While we find this metric (known as T5050: temperature where ice and liquid phases are
305 equal) to be only weakly correlated with 40-50°S SFC SWCRE across a set of 23 CMIP5/6
306 models ($r=-0.16$), it is possible that there are other unknown GCM tuning dynamics at play here.
307 Our results also suggest that the warm-cold SWCRE gradient is not useful beyond CMIP5,
308 potentially at odds with prior work (see Text S3). As past studies have noted, finding these
309 relationships is the first step to understanding them, but healthy skepticism should be maintained
310 about this EC until it is better understood (Caldwell et al. 2014; Klein and Hall, 2015). Future
311 work should seek to better understand mechanisms and the sources of model bias in SFC SWCRE
312 across the SH extratropics.

313

314 **Acknowledgements**

315 We acknowledge funding from the Regional and Global Model Analysis Program for the Office
316 of Science of the U.S. Department of Energy through the Program for Climate Model Diagnosis
317 and Intercomparison (PCMDI). The work of M. D. Zelinka and S. Po-Chedley was performed
318 under the auspices of the U.S. Department of Energy by Lawrence Livermore National
319 Laboratory under contract DE-AC52-07NA27344. We thank the World Climate Research
320 Programme's Working Group on Coupled Modeling and the individual modeling groups for their
321 roles in making CMIP data available. We also thank the two reviewers for their constructive
322 feedback.

323

324 **Open Research**

325 All data used in this study is publicly available. The CMIP output (models listed in Tables S1-S3)
326 is available from the Earth System Grid Federation (<https://aims2.llnl.gov/search>). CERES data is
327 available from: <https://ceres.larc.nasa.gov/data/>. Data from ERA5 (Hersbach et al. 2023) were
328 also used in the creation of this manuscript. The code relating to this study will be made available
329 prior to publication.

330 **References**

331 Bony, S., & Dufresne, J. L. (2005). Marine boundary layer clouds at the heart of tropical cloud
332 feedback uncertainties in climate models. *Geophysical Research Letters*, 32(20), 1–4.
333 <https://doi.org/10.1029/2005GL023851>

334 Bony, S., Colman, R., Kattsov, V. M., Allan, R. P., Bretherton, C. S., Dufresne, J. L., Hall, A.,
335 Hallegatte, S., Holland, M. M., Ingram, W., Randall, D. A., Soden, B. J., Tselioudis, G., & Webb,
336 M. J. (2006). How well do we understand and evaluate climate change feedback processes?
337 *Journal of Climate*, 19, 3445–3482. <https://doi.org/10.1175/JCLI3819.1>

338 Bowman, K. W., Cressie, N., Qu, X., & Hall, A. (2018). A Hierarchical Statistical Framework for
339 Emergent Constraints: Application to Snow-Albedo Feedback. *Geophysical Research Letters*,
340 45(23), 13,050–13,059. <https://doi.org/10.1029/2018GL080082>

341 Brient, F., & Schneider, T. (2016). Constraints on climate sensitivity from space-based
342 measurements of low-cloud reflection. *Journal of Climate*, 29(16), 5821–5835.
343 <https://doi.org/10.1175/JCLI-D-15-0897.1>

344 Brient, F., Schneider, T., Tan, Z., Bony, S., Qu, X., & Hall, A. (2016). Shallowness of tropical
345 low clouds as a predictor of climate models' response to warming. *Climate Dynamics*, 47(1–2),
346 433–449. <https://doi.org/10.1007/s00382-015-2846-0>

347 Caldwell, P. M., Bretherton, C. S., Zelinka, M. D., Klein, S. A., Santer, B. D., & Sanderson, B.
348 M. (2014). Statistical significance of climate sensitivity predictors obtained by data mining.
349 *Geophysical Research Letters*, 41(5), 1803–1808. <https://doi.org/10.1002/2014GL059205>

350 Caldwell, P. M., Zelinka, M. D., & Klein, S. A. (2018). Evaluating emergent constraints on
351 equilibrium climate sensitivity. *Journal of Climate*, 31(10), 3921–3942.
352 <https://doi.org/10.1175/JCLI-D-17-0631.1>

353 Caldwell, P. M., Zelinka, M. D., Taylor, K. E., & Marvel, K. (2016). Quantifying the sources of
354 intermodel spread in equilibrium climate sensitivity. *Journal of Climate*, 29(2), 513–524.
355 <https://doi.org/10.1175/JCLI-D-15-0352.1>

356 Cesana, G. v., & del Genio, A. D. (2021). Observational constraint on cloud feedbacks suggests
357 moderate climate sensitivity. *Nature Climate Change*, 11(3), 213–218.
358 <https://doi.org/10.1038/s41558-020-00970-y>

359 Cess, R. D., Potter, G. L., Blanchet, J. P., Boer, G. J., Genio, A. D. D., DÉ Qu É, M., Dymnikov,
360 V., Galin, V., Gates, W. L., Ghan, S. J., Kiehl, J. T., Lacis, A. A., Treut, H. le, Li, Z. X., Liang, X.
361 Z., Mc Avaney, B. J., Meleshko, V. P., Mitchell, J. F. B., Morcrette, J. J., ... Zhang, M. H.
362 (1990). Intercomparison and interpretation of climate feedback processes in 19 atmospheric

363 general circulation models. *Journal of Geophysical Research*, 95(D10).
364 <https://doi.org/10.1029/jd095id10p16601>
365 Eyring, V., Bony, S., Meehl, G. A., Senior, C. A., Stevens, B., Stouffer, R. J., & Taylor, K. E.
366 (2016). Overview of the Coupled Model Intercomparison Project Phase 6 (CMIP6) experimental
367 design and organization. *Geoscientific Model Development*, 9(5), 1937–1958.
368 <https://doi.org/10.5194/gmd-9-1937-2016>
369 Forster, P., T. Storelvmo, K. Armour, W. Collins, J.-L. Dufresne, D. Frame, D.J. Lunt, T.
370 Mauritzen, M.D. Palmer, M. Watanabe, M. Wild, and H. Zhang, The Earth's Energy Budget,
371 Climate Feedbacks, and Climate Sensitivity. In *Climate Change 2021: The Physical Science
Basis. Contribution of Working Group I to the Sixth Assessment Report of the Intergovernmental
Panel on Climate Change* [Masson-Delmotte, V., P. Zhai, A. Pirani, S.L. Connors, C. Péan, S.
373 Berger, N. Caud, Y. Chen, L. Goldfarb, M.I. Gomis, M. Huang, K. Leitzell, E. Lonnoy, J.B.R.
374 Matthews, T.K. Maycock, T. Waterfield, O. Yelekçi, R. Yu, and B. Zhou (eds.)]. Cambridge
375 University Press, Cambridge, United Kingdom and New York, NY, USA, 923–1054 (2021).
376 Gettelman, A., Hannay, C., Bacmeister, J. T., Neale, R. B., Pendergrass, A. G., Danabasoglu, G.,
377 Lamarque, J. -F., Fasullo, J. T., Bailey, D. A., Lawrence, D. M., & Mills, M. J. (2019). High
378 Climate Sensitivity in the Community Earth System Model Version 2 (CESM2). *Geophysical
Research Letters*, 46(14), 8329–8337. <https://doi.org/10.1029/2019gl083978>
379 Grise, K. M., Polvani, L. M., & Fasullo, J. T. (2015). Reexamining the relationship between
380 climate sensitivity and the Southern Hemisphere radiation budget in CMIP models. *Journal of
Climate*, 28(23), 9298–9312. <https://doi.org/10.1175/JCLI-D-15-0031.1>
381 Hall, A., Cox, P., Huntingford, C., & Klein, S. (2019). Progressing emergent constraints on future
382 climate change. *Nature Climate Change*, 9(4), 269–278. [https://doi.org/10.1038/s41558-019-0436-6](https://doi.org/10.1038/s41558-019-
383 0436-6)
384 Hersbach, H., Bell, B., Berrisford, P., Biavati, G., Horányi, A., Muñoz Sabater, J., Nicolas, J.,
385 Peubey, C., Radu, R., Rozum, I., Schepers, D., Simmons, A., Soci, C., Dee, D., Thépaut, J-N.
386 (2023). ERA5 monthly averaged data on single levels from 1940 to present. Copernicus Climate
387 Change Service (C3S) Climate Data Store (CDS) [Dataset].
388 <https://doi.org/10.24381/cds.f17050d7>
389 Hersbach, H., Bell, B., Berrisford, P., Hirahara, S., Horányi, A., Muñoz-Sabater, J., Nicolas, J.,
390 Peubey, C., Radu, R., Schepers, D., Simmons, A., Soci, C., Abdalla, S., Abellán, X., Balsamo, G.,
391 Bechtold, P., Biavati, G., Bidlot, J., Bonavita, M., ... Thépaut, J. N. (2020). The ERA5 global
392 reanalysis. *Quarterly Journal of the Royal Meteorological Society*, 146(730), 1999–2049.
393 <https://doi.org/10.1002/qj.3803>

397 Hirota, N., Ogura, T., Shiogama, H., Caldwell, P., Watanabe, M., Kamae, Y., & Suzuki, K.
398 (2021). Underestimated marine stratocumulus cloud feedback associated with overly active deep
399 convection in models. *Environmental Research Letters*, 16(7). <https://doi.org/10.1088/1748-9326/abfb9e>

400 Jiang, X., Su, H., Jiang, J. H., Neelin, J. D., Wu, L., Tsushima, Y., & Elsaesser, G. (2023). Muted
401 extratropical low cloud seasonal cycle is closely linked to underestimated climate sensitivity in
402 models. *Nature Communications*, 14(5586). <https://doi.org/10.1038/s41467-023-41360-0>

403 Kang, S. M., Ceppi, P., Yu, Y., & Kang, I. S. (2023). Recent global climate feedback controlled
404 by Southern Ocean cooling. *Nature Geoscience*, 16(9), 775–780. <https://doi.org/10.1038/s41561-023-01256-6>

405 Kang, S. M., Hawcroft, M., Xiang, B., Hwang, Y. T., Cazes, G., Codron, F., Crueger, T., Deser,
406 C., Hodnebrog, Ø., Kim, H., Kim, J., Kosaka, Y., Losada, T., Mechoso, C. R., Myhre, G., Seland,
407 Ø., Stevens, B., Watanabe, M., & Yu, S. (2019). Extratropical–tropical interaction model
408 intercomparison project (ETIN-MIP): Protocol and initial results. *Bulletin of the American
409 Meteorological Society*, 100(12), 2589–2605. <https://doi.org/10.1175/BAMS-D-18-0301.1>

410 Kang, S. M., Xie, S.-P., Shin, Y., Kim, H., Hwang, Y.-T., Stuecker, M. F., Xiang, B., &
411 Hawcroft, M. (2020). Walker circulation response to extratropical radiative forcing. *Science
412 Advances*, 6.

413 Kato, S., Rose, F. G., Rutan, D. A., Thorsen, T. J., Loeb, N. G., Doelling, D. R., Huang, X.,
414 Smith, W. L., Su, W., & Ham, S. H. (2018). Surface irradiances of edition 4.0 Clouds and the
415 Earth’s Radiant Energy System (CERES) Energy Balanced and Filled (EBAF) data product.
416 *Journal of Climate*, 31(11), 4501–4527. <https://doi.org/10.1175/JCLI-D-17-0523.1>

417 Kay, J. E., Bourdages, L., Miller, N. B., Morrison, A., Yettella, V., Chepfer, H., & Eaton, B.
418 (2016). Evaluating and improving cloud phase in the Community Atmosphere Model version 5
419 using spaceborne lidar observations. *Journal of Geophysical Research: Atmospheres*, 1–19.
420 <https://doi.org/10.1002/2014JD022994>. Received

421 Klein, S. A., & Hall, A. (2015). Emergent Constraints for Cloud Feedbacks. *Current Climate
422 Change Reports*, 1(4), 276–287. <https://doi.org/10.1007/s40641-015-0027-1>

423 Klein, S. A., Zhang, Y., Zelinka, M. D., Pincus, R., Boyle, J., & Gleckler, P. J. (2013). Are
424 climate model simulations of clouds improving? An evaluation using the ISCCP simulator.
425 *Journal of Geophysical Research Atmospheres*, 118(3), 1329–1342.
426 <https://doi.org/10.1002/jgrd.50141>

429 Lauer, A., Bock, L., Hassler, B., Schröder, M., & Stengel, M. (2023). Cloud Climatologies from
430 Global Climate Models-A Comparison of CMIP5 and CMIP6 Models with Satellite Data. *Journal*
431 *of Climate*, 36(2), 281–311. <https://doi.org/10.1175/JCLI-D-22-0181.1>

432 Lauer, A., & Hamilton, K. (2013). Simulating clouds with global climate models: A comparison
433 of CMIP5 results with CMIP3 and satellite data. *Journal of Climate*, 26(11), 3823–3845.
434 <https://doi.org/10.1175/JCLI-D-12-00451.1>

435 Lipat, B. R., Tselioudis, G., Grise, K. M., & Polvani, L. M. (2017). CMIP5 models' shortwave
436 cloud radiative response and climate sensitivity linked to the climatological Hadley cell extent.
437 *Geophysical Research Letters*, 44(11), 5739–5748. <https://doi.org/10.1002/2017GL073151>

438 Loeb, N. G., Doelling, D. R., Wang, H., Su, W., Nguyen, C., Corbett, J. G., Liang, L., Mitrescu,
439 C., Rose, F. G., & Kato, S. (2018). Clouds and the Earth's Radiant Energy System (CERES)
440 Energy Balanced and Filled (EBAF) top-of-atmosphere (TOA) edition-4.0 data product. *Journal*
441 *of Climate*, 31(2), 895–918. <https://doi.org/10.1175/JCLI-D-17-0208.1>

442 Lutsko, N. J., Popp, M., Nazarian, R. H., & Albright, A. L. (2021). Emergent Constraints on
443 Regional Cloud Feedbacks. *Geophysical Research Letters*, 48(10).
444 <https://doi.org/10.1029/2021GL092934>

445 McCoy, D. T., Field, P., Bodas-Salcedo, A., Elsaesser, G. S., & Zelinka, M. D. (2020). A
446 Regime-Oriented Approach to Observationally Constraining Extratropical Shortwave Cloud
447 Feedbacks. *Journal of Climate*, 33(23), 9967–9983. <https://doi.org/10.1175/jcli-d-19-0987.1>

448 McCoy, D. T., Tan, I., Hartmann, D. L., Zelinka, M. D., & Storelvmo, T. (2016). On the
449 relationships among cloud cover, mixed-phase partitioning, and planetary albedo in GCMs.
450 *Journal of Advances in Modeling Earth Systems*, 8(2), 650–668.
451 <https://doi.org/10.1002/2015MS000589>

452 Mechoso, C. R., Losada, T., Koseki, S., Mohino-Harris, E., Keenlyside, N., Castaño-Tierno, A.,
453 Myers, T. A., Rodriguez-Fonseca, B., & Toniazzo, T. (2016). Can reducing the incoming energy
454 flux over the Southern Ocean in a CGCM improve its simulation of tropical climate? *Geophysical*
455 *Research Letters*, 43(20), 11,057-11,063. <https://doi.org/10.1002/2016GL071150>

456 Meehl, G. A., Covey, C., Delworth, T., Latif, M., McAvaney, B., Mitchell, J. F. B., Stouffer, R.
457 J., & Taylor, K. E. (2007). The WCRP CMIP3 multimodel dataset: A new era in climatic change
458 research. *Bulletin of the American Meteorological Society*, 88(9), 1383–1394.
459 <https://doi.org/10.1175/BAMS-88-9-1383>

460 Myers, T. A., & Norris, J. R. (2016). Reducing the uncertainty in subtropical cloud feedback.
461 *Geophysical Research Letters*, 43(5), 2144–2148. <https://doi.org/10.1002/2015GL067416>

462 Myers, T. A., Scott, R. C., Zelinka, M. D., Klein, S. A., Norris, J. R., & Caldwell, P. M. (2021).
463 Observational constraints on low cloud feedback reduce uncertainty of climate sensitivity. *Nature*
464 *Climate Change*, 11(6), 501–507. <https://doi.org/10.1038/s41558-021-01039-0>

465 Nam, C., Bony, S., Dufresne, J. L., & Chepfer, H. (2012). The too few, too bright tropical low-
466 cloud problem in CMIP5 models. *Geophysical Research Letters*, 39(21).
467 <https://doi.org/10.1029/2012GL053421>

468 Qu, X., Hall, A., Klein, S. A., & Caldwell, P. M. (2014). On the spread of changes in marine low
469 cloud cover in climate model simulations of the 21st century. *Climate Dynamics*, 42(9–10), 2603–
470 2626. <https://doi.org/10.1007/s00382-013-1945-z>

471 Qu, X., Hall, A., Klein, S. A., & Deangelis, A. M. (2015). Positive tropical marine low-cloud
472 cover feedback inferred from cloud-controlling factors. *Geophysical Research Letters*, 42(18),
473 7767–7775. <https://doi.org/10.1002/2015GL065627>

474 Schlund, M., Lauer, A., Gentine, P., Sherwood, S. C., & Eyring, V. (2020). Emergent constraints
475 on equilibrium climate sensitivity in CMIP5: Do they hold for CMIP6? *Earth System Dynamics*,
476 11(4), 1233–1258. <https://doi.org/10.5194/esd-11-1233-2020>

477 Shell, K. M., Kiehl, J. T., & Shields, C. a. (2008). Using the radiative kernel technique to
478 calculate climate feedbacks in NCAR's Community Atmospheric Model. *Journal of Climate*, 21,
479 2269–2282. <https://doi.org/10.1175/2007JCLI2044.1>

480 Sherwood, S., Webb, M. J., Annan, J. D., Armour, K. C., Forster, P. M., Hargreaves, J. C.,
481 Hegerl, G., Klein, S. A., Marvel, K. D., Rohling, E. J., Watanabe, M., Andrews, T., Braconnot, P.,
482 Bretherton, C. S., Foster, G. L., Hausfather, Z., Heydt, A. S. von der, Knutti, R., Mauritzen, T., ...
483 Zelinka, M. D. (2020). An assessment of Earth's climate sensitivity using multiple lines of
484 evidence. *Reviews of Geophysics*, 58, e2019RG000678. <https://doi.org/10.1029/2019RG000678>

485 Siler, N., Po-Chedley, S., & Bretherton, C. S. (2018). Variability in modeled cloud feedback tied
486 to differences in the climatological spatial pattern of clouds. *Climate Dynamics*, 50(3–4), 1209–
487 1220. <https://doi.org/10.1007/s00382-017-3673-2>

488 Soden, B. J., Held, I. M., Colman, R. C., Shell, K. M., Kiehl, J. T., & Shields, C. a. (2008).
489 Quantifying climate feedbacks using radiative kernels. *Journal of Climate*, 21(1988), 3504–3520.
490 <https://doi.org/10.1175/2007JCLI2110.1>

491 Taylor, K. E., Stouffer, R. J., & Meehl, G. A. (2012). An Overview of CMIP5 and the Experiment
492 Design. *Bulletin of the American Meteorological Society*, 3(April), 485–498.
493 <https://doi.org/10.1175/BAMS-D-11-00094.1>

494 Terai, C. R., Klein, S. A., & Zelinka, M. D. (2016). Constraining the low-cloud optical depth
495 feedback at middle and high latitudes using satellite observations. *Journal of Geophysical*
496 *Research*, 121(16), 9696–9716. <https://doi.org/10.1002/2016JD025233>

497 Tian, B. (2015). Spread of model climate sensitivity linked to double-Intertropical Convergence
498 Zone bias. *Geophysical Research Letters*, 42(10), 4133–4141.
499 <https://doi.org/10.1002/2015GL064119>

500 Trenberth, K. E., & Fasullo, J. T. (2010). Simulation of present-day and twenty-first-century
501 energy budgets of the southern oceans. *Journal of Climate*, 23(2), 440–454.
502 <https://doi.org/10.1175/2009JCLI3152.1>

503 Vignesh, P. P., Jiang, J. H., Kishore, P., Su, H., Smay, T., Brighton, N., & Velicogna, I. (2020).
504 Assessment of CMIP6 Cloud Fraction and Comparison with Satellite Observations. *Earth and*
505 *Space Science*, 7(2). <https://doi.org/10.1029/2019EA000975>

506 Volodin, E. M. (2008). Relation between temperature sensitivity to doubled carbon dioxide and
507 the distribution of clouds in current climate models. *Izvestiya, Atmospheric and Oceanic Physics*,
508 44(3), 288–299. <https://doi.org/10.1134/S0001433808030043>

509 Wall, C. J., Storelvmo, T., Norris, J. R., & Tan, I. (2022). Observational Constraints on Southern
510 Ocean Cloud-Phase Feedback. *Journal of Climate*, 35, 5087–5102. <https://doi.org/10.1175/JCLI-D-21>

512 Webb, M. J., Lambert, F. H., & Gregory, J. M. (2013). Origins of differences in climate
513 sensitivity, forcing and feedback in climate models. *Climate Dynamics*, 40(3–4), 677–707.
514 <https://doi.org/10.1007/s00382-012-1336-x>

515 Webb, M. J., & Lock, A. P. (2020). Testing a Physical Hypothesis for the Relationship Between
516 Climate Sensitivity and Double-ITCZ Bias in Climate Models. *Journal of Advances in Modeling*
517 *Earth Systems*, 12. <https://doi.org/10.1029/2019MS001999>

518 Williams, K. D., & Tselioudis, G. (2007). GCM intercomparison of global cloud regimes:
519 Present-day evaluation and climate change response. *Climate Dynamics*, 29(2–3), 231–250.
520 <https://doi.org/10.1007/s00382-007-0232-2>

521 Williamson, M. S., Thackeray, C. W., Cox, P. M., Hall, A., Huntingford, C., & Nijssse, F. J. M. M.
522 (2021). Emergent constraints on climate sensitivities. *Reviews of Modern Physics*, 93(2), 025004.
523 <https://doi.org/10.1103/RevModPhys.93.025004>

524 Zelinka, M. D., Myers, T. A., McCoy, D. T., Po-Chedley, S., Caldwell, P. M., Ceppli, P., Klein, S.
525 A., & Taylor, K. E. (2020). Causes of Higher Climate Sensitivity in CMIP6 Models. *Geophysical*
526 *Research Letters*, 47(1), e2019GL085782. <https://doi.org/10.1029/2019GL085782>

527 Zhai, C., Jiang, J. H., & Su, H. (2015). Long-term cloud change imprinted in seasonal cloud
528 variation: More evidence of high climate sensitivity. *Geophysical Research Letters*, 42(20),
529 8729–8737. <https://doi.org/10.1002/2015GL065911>

530 Zhou, C., Zelinka, M. D., Dessler, A. E., & Klein, S. A. (2015). The relationship between
531 interannual and long-term cloud feedbacks. *Geophysical Research Letters*, 42(23), 10463–10469.
532 <https://doi.org/10.1002/2015GL066698>

533 Zhou, W., Leung, L. R., Siler, N., & Lu, J. (2023). Future precipitation increase constrained by
534 climatological pattern of cloud effect. *Nature Communications*, 14(1), 6363.
535 <https://doi.org/10.1038/s41467-023-42181-x>

536 Zhu, J., Otto-Bliesner, B. L., Brady, E. C., Gettelman, A., Bacmeister, J. T., Neale, R. B.,
537 Poulsen, C. J., Shaw, J. K., McGraw, Z. S., & Kay, J. E. (2022). LGM Paleoclimate Constraints
538 Inform Cloud Parameterizations and Equilibrium Climate Sensitivity in CESM2. *Journal of*
539 *Advances in Modeling Earth Systems*, 14(4). <https://doi.org/10.1029/2021MS002776>

540